

Laminar Superlayer at the Turbulence Boundary

M. Holzner^{1,*} and B. Lüthi²

¹Max Planck Institute for Dynamics and Self-Organisation, Bunsenstr. 10, 37073 Göttingen, Germany

²Institute of Environmental Engineering, ETH Zurich, 8093 Zurich, Switzerland

(Received 19 July 2010; published 31 March 2011)

In this Letter we present results from particle tracking velocimetry and direct numerical simulation that are congruent with the existence of a laminar superlayer, as proposed in the pioneering work of Corrsin and Kistler (NACA, Technical Report No. 1244, 1955). We find that the local superlayer velocity is dominated by a viscous component and its magnitude is comparable to the characteristic velocity of the smallest scales of motion. This slow viscous process involves a large surface area so that the global rate of turbulence spreading is set by the largest scales of motion. These findings are important for a better understanding of mixing of mass and momentum in a variety of flows where thin layers of shear exist. Examples are boundary layers, clouds, planetary atmospheres, and oceans.

DOI: 10.1103/PhysRevLett.106.134503

PACS numbers: 47.27.wj, 47.53.+n, 68.05.-n

Sharp and strongly contorted interfaces are known to exist at the outer boundary of free-shear turbulent flows such as turbulent jets, wakes, and mixing layers, where they separate the turbulent from the irrotational ambient flow regions. These interfaces fluctuate vigorously and are convoluted by the motion of turbulent eddies, while at the same time they advance relative to the fluid as a result of the small-scale entrainment process [1]. For example, in combustion processes flames are often thin and located at the turbulence boundary, e.g., [2], so that the behavior of interfaces affects local rates of mixing of heat and species. Thin shear layers also play an important role at the boundary of clouds in the atmosphere, where there are sharp inhomogeneous fronts bounding the turbulent cloud interior from dry air surrounding it, e.g., [3,4]. They also form in planetary atmospheres, e.g., so-called “potential vorticity (PV) staircases” on Jupiter [5] and in zonal jets in Earth’s crust, e.g., [6].

In their pioneering work, Corrsin and Kistler [7] suggested that the interface between turbulent and irrotational regions is characterized by the existence of a thin layer—the so-called “laminar superlayer”—where viscosity was inferred to play an important role. In particular, they postulated that the thickness of this layer and its propagation speed are determined by molecular viscosity ν and the rate of straining of the flow, which is proportional to ϵ/ν , where $\epsilon = 2\nu s_{ij}s_{ij}$ is the energy dissipation attributed to small-scale eddies and s_{ij} are the components of the fluctuating rate of strain tensor. This would imply that the process of transfer of vorticity is due to the smallest scales of motion and independent of the large-scale motions that convolute the interface. This idea of statistical independence of large- and small-scale motions lies at the heart of the theory of local similarity in turbulence. On dimensional grounds it follows that the thickness of the interface should be proportional to the Kolmogorov length scale $\eta = (\nu^3/\epsilon)^{1/4}$, and its speed of advance, the local entrainment velocity,

should be given by the Kolmogorov velocity $u_\eta = (\epsilon\nu)^{1/4}$, respectively. The results of recent numerical [8,9] and experimental [10,11] studies on flows characterized by significant mean shear showed evidence that the viscous eddies are indeed important for the spreading of the interface (small-scale “nibbling”), but find that the length scale for the associated average thickness is the Taylor length scale $\bar{\lambda} = \{\overline{u_1^2}/(\overline{\partial u_1/\partial x_1})^2\}^{1/2}$ rather than $\bar{\eta} = (\nu^3/\bar{\epsilon})^{1/4}$ [8–11], where the overbar denotes the average value. This was attributed to the thickness of the turbulent-nonturbulent interface, a layer that is supposed to be containing the laminar superlayer [8]. The influence of mean shear on the dynamics of this interface is also discussed based on theoretical and experimental findings in Ref. [11], where it is argued that the strong mean shear might be responsible for a larger thickness. In a flow without mean shear, Holzner *et al.* [12,13] found that fluid parcels cross a thin layer characterized by $\bar{\eta}$ within a time characterized by the Kolmogorov time, $\bar{\tau}_\eta = (\nu/\bar{\epsilon})^{1/2}$. From these results the authors indirectly concluded that the characteristic velocity scale for the local velocity of this layer relative to the fluid is \bar{u}_η [13]. On the other hand, it is well known that, globally, the entrainment rate and the propagation velocity of the interface relative to the fluid are independent of viscosity and set by the large-scale flow parameters only, e.g., [1,14,15] and references therein. This implies that the small-scale process must somehow be accelerated through a mechanism that involves a larger range of eddy sizes [1].

In this Letter we derive an expression for the local spreading velocity v_n , which allows us to test for Corrsin and Kistler’s postulate in a direct way. The presented experimental and numerical results underline the importance of viscous effects for the outward spreading of the interface and show that velocity and thickness are determined by the viscous eddies, which are on the order of the

Kolmogorov velocity and length scale, respectively. We found that the viscous outward spreading is determined by the superlayer curvature and the concavity of the vorticity profile normal to the superlayer, the latter effect being dominant.

We conducted experiments by using particle tracking velocimetry (PTV) in scanning mode, a method that allows measuring the velocity of tracer particles that are passively advected by the flow based on stereoscopic high speed imaging [16]. Turbulence is forced by a planar grid [13] with 4 mm mesh size and 1 mm rod diameter installed near the upper edge of a water-filled glass tank and oscillating at a frequency of 6 Hz and an amplitude of 4 mm. When the grid motion is started, a turbulent flow region develops and spreads through entrainment of surrounding irrotational fluid. The size of the observation volume is about $2 \times 1.5 \times 1.5 \text{ cm}^3$ and is located about 2 cm below the grid. The number of tracked particles is about 6×10^3 per volume scan at a scanning rate of 50 Hz. The trajectories were processed to calculate the three components of the velocity u_i , Lagrangian acceleration a_i , and their gradients [13]. The Reynolds number is $\text{Re} \approx 1000$ corresponding to a Taylor microscale Reynolds number $\text{Re}\lambda \approx 50$ and the results are compared to a numerical simulation at the same Reynolds number. Direct numerical simulations (DNSs) were performed in a box of fluid initially at rest [13] with $\text{Re} = (1-4) \times 10^3$. Random (in space and time) velocity perturbations are applied at the boundary $x_2 = 0$. The Navier-Stokes equations are solved with a finite differences scheme and with time advancement computed by a semi-implicit Runge-Kutta method. The resolution is $256 \times 256 \times 256$ grid points in x_1 , x_2 , and x_3 direction.

In both experiment and simulation, the turbulence boundary is detected by using a threshold on enstrophy $\omega^2 = \boldsymbol{\omega} \cdot \boldsymbol{\omega}$, where $\boldsymbol{\omega}$ is the vorticity vector, e.g., [8,10,12]. The selected value of the threshold is 5% of the mean enstrophy in the turbulent region. Figure 1 shows a snapshot of the isosurface obtained from DNS, and it can

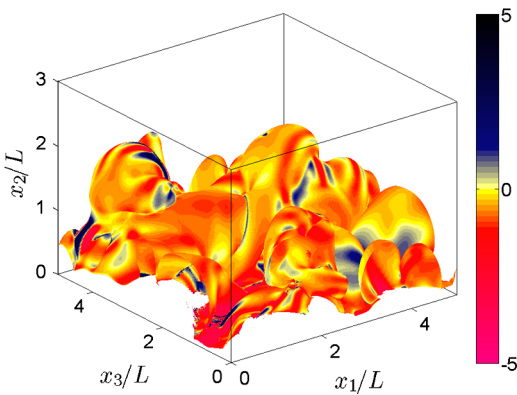


FIG. 1 (color online). Snapshot of the propagation velocity v_n normalized by \bar{u}_η rendered over an enstrophy isosurface from DNS at $\text{Re}_\lambda = 50$.

be seen that the convoluted surface is characterized by rather smooth bulges with sharper ridges in between. When considering the evolution of this isosurface in time, it is convenient to separate between the advection due to the underlying flow field and its velocity relative to the fluid. We write the velocity of an isosurface element, \mathbf{u}^s , as a sum of fluid velocity, \mathbf{u} , and velocity of the area element relative to the fluid, $\mathbf{V} = v_n \hat{\mathbf{n}}$, that is, $\mathbf{u}^s = \mathbf{u} + \mathbf{V}$, where $\hat{\mathbf{n}} = \nabla \omega^2 / |\nabla \omega^2|$ is the surface normal and v_n is the normal velocity component. By definition the total change of ω^2 in the frame of reference moving with an enstrophy isosurface element will be zero, and this is used in the following to derive a relation for the propagation velocity:

$$\frac{D^s \omega^2}{D^s t} = \frac{\partial \omega^2}{\partial t} + u_j^s \frac{\partial \omega^2}{\partial x_j} = \frac{\partial \omega^2}{\partial t} + (u_j + V_j) \frac{\partial \omega^2}{\partial x_j} = 0. \quad (1)$$

The isosurface will hence evolve according to the relation

$$\frac{\partial \omega^2}{\partial t} + u_j \frac{\partial \omega^2}{\partial x_j} = -V_j \frac{\partial \omega^2}{\partial x_j} = -v_n |\nabla \omega^2|. \quad (2)$$

With the use of the enstrophy transport equation,

$$\frac{\partial \omega^2/2}{\partial t} + u_j \frac{\partial \omega^2/2}{\partial x_j} = \omega_i \omega_j s_{ij} + \nu \omega_i \nabla^2 \omega_i, \quad (3)$$

we obtain a relation for v_n , written as a sum of an inviscid and a viscous contribution:

$$v_n = -\frac{2\omega_i \omega_j s_{ij}}{|\nabla \omega^2|} - \frac{2\nu \omega_i \nabla^2 \omega_i}{|\nabla \omega^2|} = v_n^{\text{inv}} + v_n^{\text{vis}}. \quad (4)$$

A snapshot of the distribution of v_n normalized by \bar{u}_η , where the overbar denotes the average over the locations of the isosurface, is shown in Fig. 1. The probability density functions (PDFs) of v_n^{inv} , v_n^{vis} and v_n evaluated at the isosurface locations are depicted in Fig. 2, and it appears that all distributions have a negative skewness. A negative velocity points towards the irrotational region; i.e., the turbulent region expands. The figure shows that the inviscid contribution is small and v_n is dominated by the viscous term. Both the mean values and the standard deviations of v_n are close to \bar{u}_η . Experiment and simulation show good qualitative agreement, where the PDF of v_n^{inv} from the experiment displays a somewhat higher skewness compared to the respective curve from DNS (Fig. 2). The qualitative trends do not change for a wide range of isovalues in the numerics; in the experiment only one decade, $(0.01-0.1)\langle \omega^2 \rangle$, could be tested due to the influence of noise at very low values [12]. From the numerical data we calculated the balance between global and integral volume flux, e.g., [9,17,18]. The ratio between the volume flux, $Q = \int v_n dA$, integrated over the convoluted area of the isosurface and the global value, $Q_0 = u_e A_0$, is shown in the inset of Fig. 2 for different thresholds and

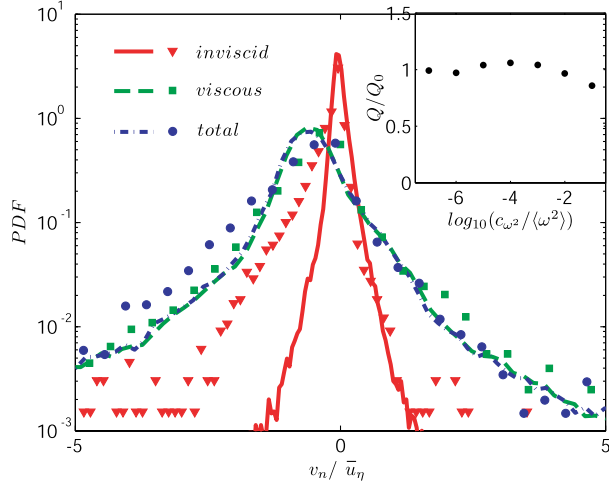


FIG. 2 (color online). PDFs of the inviscid (solid red line, ∇), viscous (dashed green line, \square) and total (dash-dotted blue line, \circ) propagation velocity. Lines are from DNS, symbols from PTV. The inset shows the ratio between the integrated and global volume flux for different threshold values c_{ω^2} normalized with the mean enstrophy in the turbulent region (DNS only).

yields 1 ± 0.07 , where $A_0 = 25L^2$ is the cross-sectional area of the computational domain, $u_e = dH(t)/dt$ is the entrainment velocity, and $H(t)$ is the cross-sectional average of the isosurface positions at time t . This shows that the turbulent flow strongly deforms the superlayer to account for the same volume flux with a large surface area and a small characteristic velocity. Given that the viscous term dominates v_n it is natural to define the associated local length scale as $\delta = \nu/v_n$, and this yields values for the superlayer thickness close to $\bar{\eta}$. The prediction of [7] would imply that $\bar{\delta}/\bar{\eta} \approx \text{const}$ and $\bar{\delta}/\bar{\lambda} \propto \text{Re}^{-1/4}$. In contrast, if $\bar{\delta} \propto \bar{\lambda}$, then $\bar{\delta}/\bar{\eta} \propto \text{Re}^{1/4}$ and $\bar{\delta}/\bar{\lambda} = \text{const}$. Simulations up to $\text{Re} = 4000$ show that $\bar{\delta}/\bar{\eta}$ is rather close to a horizontal trend, i.e., $\bar{\delta}/\bar{\eta} \approx \text{const}$ and does not follow $\text{Re}^{1/4}$, and, analogously, the ratio $\bar{\delta}/\bar{\lambda}$ does not show a horizontal trend and is rather close to $\text{Re}^{-1/4}$ (Fig. 3). We have hence identified a viscous superlayer, where viscosity is mostly responsible for the local advancement relative to the fluid and towards the irrotational ambient flow, as

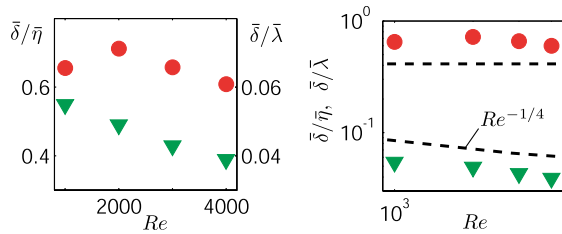


FIG. 3 (color online). Mean superlayer thickness $\bar{\delta}$ normalized with $\bar{\eta}$ (\circ) and $\bar{\lambda}$ (∇) as a function of Reynolds number on linear (left) and logarithmic axes (right). The dashed lines show the slopes Re^0 and $\text{Re}^{-1/4}$, DNS only.

postulated in [7]. In Fig. 4 (top, left) we plot the PDF of the cosine of the angle between $\boldsymbol{\omega}$ and the isosurface normal $\hat{\mathbf{n}}$. Since vortex lines cannot end in the irrotational region, the vorticity component normal to the surface must vanish at the superlayer, so that the vorticity vector is oriented tangentially and the value of the cosine is concentrated at zero. Consistent with the negative skewness of the PDF of v_n^{inv} shown in Fig. 2, straining motion is mostly stretching the vorticity at the superlayer [12] and the intermediate eigenvector $\boldsymbol{\lambda}_2$ of the rate of strain tensor is mostly oriented tangentially, while the compressive eigenvector $\boldsymbol{\lambda}_3$ is mostly oriented normally to the laminar superlayer, respectively (Fig. 4 top, right). Predominant vortex stretching thus appears to be one of the reasons why the turbulence boundary remains sharp despite the fact that viscosity keeps diffusing it. Figure 4 depicts joint PDFs of the spreading velocity v_n and the local Kolmogorov velocity u_η obtained from DNS (bottom, left) and PTV (bottom, right). The isoprobability contours are not aligned with the diagonal, which implies that there is no pointwise correlation between the two quantities and the local similarity hypothesis does not hold. This poses the question of what determines then the local viscous spreading velocity towards the irrotational flow region.

It is useful to decompose the term $\nu \omega_i \nabla^2 \omega_i$ into the sum of the divergence of a flux term $\nu \nabla \cdot (\nabla \omega^2/2)$ (viscous diffusion of enstrophy) and a purely negative term $-\nu \nabla \omega_i \cdot \nabla \omega_i$ (viscous destruction of enstrophy), e.g., [14], which yields

$$v_n^{\text{vis}} = -\frac{\nu \nabla \cdot (\nabla \omega^2)}{|\nabla \omega^2|} + \frac{2\nu \nabla \omega_i \cdot \nabla \omega_i}{|\nabla \omega^2|}. \quad (5)$$

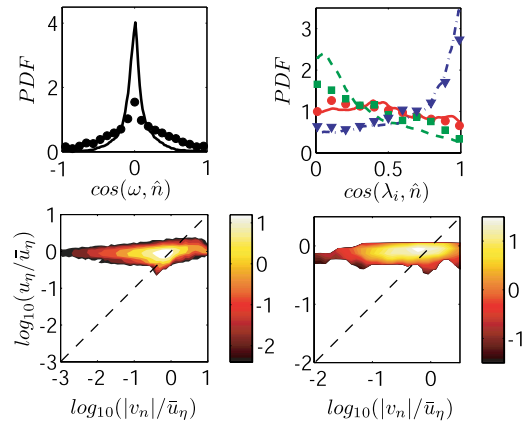


FIG. 4 (color online). Top: PDF of the cosine of the angle between vorticity and the surface normal (left) and PDF of the absolute value of the cosine of the angle between the eigenvectors of the rate of strain tensor and the surface normal (right), (solid red line, \circ) $i = 1$, (dashed green line, \square) $i = 2$, (dash-dotted blue line, ∇) $i = 3$. Lines are from DNS, symbols from PTV. Bottom: Joint PDF of v_n versus the local Kolmogorov velocity from DNS (left) and PTV (right). The scale of the color bars is logarithmic.

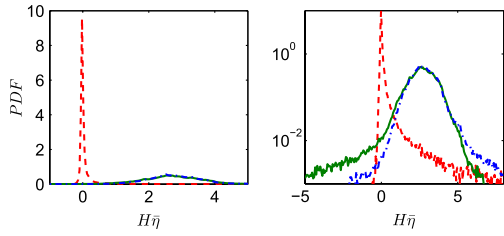


FIG. 5 (color online). PDFs of the mean curvature H_m (dashed red line), normal diffusion term H_n (solid green line), and the sum $2H_m + H_n$ (dash-dotted blue line) on linear (left) and semilogarithmic axis (right), DNS only.

Operating on the first term one obtains

$$\mathbf{v}_n^{\text{vis}} = -\nu(\nabla \cdot \hat{\mathbf{n}}) - \frac{\nu \hat{\mathbf{n}} \cdot \nabla(|\nabla \omega^2|)}{|\nabla \omega^2|} + \frac{2\nu \nabla \omega_i \cdot \nabla \omega_i}{|\nabla \omega^2|}, \quad (6)$$

and, with x_n denoting the coordinate normal to the superlayer, finally we get

$$\mathbf{v}_n^{\text{vis}} = -\nu(\nabla \cdot \hat{\mathbf{n}}) - \frac{\nu(\partial^2 \omega^2 / \partial x_n^2)}{\partial \omega^2 / \partial x_n} + \frac{2\nu \nabla \omega_i \cdot \nabla \omega_i}{|\nabla \omega^2|}. \quad (7)$$

The last term on the right-hand side is always positive and does not contribute to the outward spreading of the superlayer. The first term is the velocity induced by the curvature of the superlayer, since the mean curvature is defined as $H_m = \nabla \cdot \hat{\mathbf{n}}/2$. Parts of the superlayer ($\nabla \cdot \hat{\mathbf{n}} > 0$) convex towards $\hat{\mathbf{n}}$ contribute to the outward velocity. The second term of Eq. (7) involves the one-dimensional local profile of $\omega^2(x_n)$ normal to the superlayer. A concave profile (approaching zero asymptotically) will contribute to the outward spreading. We refer to the term $H_n = (\partial^2 \omega^2 / \partial x_n^2) / (\partial \omega^2 / \partial x_n)$ as normal diffusion term. Figure 5 shows PDFs of the mean curvature and normal diffusion term normalized with the Kolmogorov length scale. The mean curvature H_m has a pronounced positive tail, which is mostly related to sharp ridges between bulges, whereas its median is about $-0.02\bar{\eta}^{-1}$, which corresponds to a curvature radius on the order L , and identifies smooth outward facing bulges as a dominant shape. The positive tail implies that the superlayer is strongly deformed and sharp ridges can contribute significantly to the outwards propagation velocity and counteract $H_n < 0$ events. The contribution from the normal diffusion term, however, has typically higher positive values than H_m (Fig. 5). We thus conclude that the viscous outward spreading velocity originates mostly from the concavity of the local enstrophy profile normal to the superlayer, while the effect of the curvature of the superlayer is typically smaller. Analogously, the characteristic thickness δ is mostly given by H_n^{-1} .

In summary, we measured that the local superlayer velocity, \mathbf{v}_n , is on the order of the smallest velocity scale

of the flow, namely, the Kolmogorov velocity, \bar{u}_η , and its thickness is on the order of $\bar{\eta}$. On the other hand, globally, the interface propagates with a velocity that is independent of the viscosity and on the order of the integral velocity scale [18]. We reconcile the two at first conflicting findings by showing that the superlayer area is strongly deformed by the turbulent eddies to account for the same global entrainment flux with a small characteristic velocity. The deformation of the superlayer results in strong mean curvature which is one driving factor for the outward spreading of turbulence. The dominant effect is the concavity of the local enstrophy profile normal to the superlayer. The weak pointwise correspondence between \mathbf{v}_n and \bar{u}_η invalidates the local similarity principle.

The results have implications for models which use similarity arguments [19] and make simplifying assumptions about the shape of the superlayer, which range from being flat [20] over simple shapes [19] to fractal geometries [17].

The authors acknowledge fruitful discussions with Dr. B. Hof.

*markus.holzner@ds.mpg.de

- [1] A. A. Townsend, *The Structure of Turbulent Shear Flow* (Cambridge University Press, London, 1956).
- [2] J. P. Mellado, L. Wang, and N. Peters, *J. Fluid Mech.* **626**, 333 (2009).
- [3] B. Stevens, *Annu. Rev. Earth Planet Sci.* **33**, 605 (2005).
- [4] E. Bodenschatz *et al.*, *Science* **327**, 970 (2010).
- [5] M. P. Baldwin *et al.*, *Science* **315**, 467 (2007).
- [6] T. Miyagoshi, A. Kageyama, and T. Sato, *Nature (London)* **463**, 793 (2010).
- [7] S. Corrsin and A. L. Kistler, NACA Technical Report No. TR-1244, 1955, p. 1033.
- [8] D. K. Bisset, J. C. R. Hunt, and M. M. Rogers, *J. Fluid Mech.* **451**, 383 (2002).
- [9] J. Mathew and A. J. Basu, *Phys. Fluids* **14**, 2065 (2002); C. B. DaSilva and J. C. F. Ferreira, *Phys. Fluids* **20**, 055101 (2008).
- [10] J. Westerweel *et al.*, *Phys. Rev. Lett.* **95**, 174501 (2005).
- [11] J. Westerweel *et al.*, *J. Fluid Mech.* **631**, 199 (2009).
- [12] M. Holzner *et al.*, *Phys. Fluids* **19**, 071702 (2007).
- [13] M. Holzner *et al.*, *J. Fluid Mech.* **598**, 465 (2008).
- [14] A. Tsinober, *An Informal Conceptual Introduction to Turbulence* (Springer, Berlin, 2009).
- [15] D. J. Tritton, *Physical Fluid Dynamics* (Clarendon, Gloucestershire, 1988).
- [16] K. Hoyer *et al.*, *Exp. Fluids* **39**, 923 (2005).
- [17] K. R. Sreenivasan, R. Ramshakar, and C. Meneveau, *Proc. R. Soc. A* **421**, 79 (1989).
- [18] A. Liberzon *et al.*, *Phys. Fluids* **21**, 035107 (2009).
- [19] O. M. Phillips, *J. Fluid Mech.* **51**, 97 (1972).
- [20] O. M. Phillips, *Proc. Cambridge Philos. Soc.* **51**, 220 (1955).